IOPscience iopscience.iop.org

Home Search Collections Journals About Contact us My IOPscience

Trends in elasticity and electronic structure of 5d transition metal diborides: first-principles calculations

This article has been downloaded from IOPscience. Please scroll down to see the full text article.

2007 J. Phys.: Condens. Matter 19 196212

(http://iopscience.iop.org/0953-8984/19/19/196212)

View the table of contents for this issue, or go to the journal homepage for more

Download details:
IP Address: 129.252.86.83
The article was downloaded on 28/05/2010 at 18:44

Please note that terms and conditions apply.

IOP PUBLISHING JOURNAL OF PHYSICS: CONDENSED MATTER

J. Phys.: Condens. Matter **19** (2007) 196212 (15pp) doi:10.1088/0953-8984/19/19/196212

Trends in elasticity and electronic structure of 5d transition metal diborides: first-principles calculations

Xianfeng Hao[1,2], Zhijian Wu[1], Yuanhui Xu[3], Defeng Zhou[3], Xiaojuan Liu[1] and Jian Meng[1,4]

[1] Key Laboratory of Rare Earth Chemistry and Physics, Changchun Institute of Applied Chemistry, Chinese Academy of Sciences, Changchun 130022, People's Republic of China
[2] Graduate School, Chinese Academy of Sciences, Beijing 100049, People's Republic of China
[3] School of Biological Engineering, Changchun University of Technology, Changchun 130012, People's Republic of China

E-mail: jmeng@ciac.jl.cn

Received 28 December 2006, in final form 29 March 2007
Published 19 April 2007
Online at stacks.iop.org/JPhysCM/19/196212

Abstract

We investigate the cohesive energy, heat of formation, elastic constant and electronic band structure of transition metal diborides TMB_2 (TM = Hf, Ta, W, Re, Os and Ir, Pt) in the *Pmmn* space group using the *ab initio* pseudopotential total energy method. Our calculations indicate that there is a relationship between elastic constant and valence electron concentration (VEC): the bulk modulus and shear modulus achieve their maximum when the VEC is in the range of 6.8–7.2. In addition, trends in the elastic constant are well explained in terms of electronic band structure analysis, e.g., occupation of valence electrons in states near the Fermi level, which determines the cohesive energy and elastic properties. The maximum in bulk modulus and shear modulus is attributed to the nearly complete filling of TM d–B p bonding states without filling the antibonding states. On the basis of the observed relationship, we predict that alloying W and Re in the orthorhombic structure OsB_2 might be harder than alloying the Ir element. Indeed, the further calculations confirmed this expectation.

(Some figures in this article are in colour only in the electronic version)

1. Introduction

Ultra-incompressible, superhard materials are of utmost importance due to the unusual combination of outstanding properties such as high elastic modulus and hardness, scratch resistance as well as surface durability and chemical stability. Intensive experimental and

[4] Author to whom any correspondence should be addressed.

 © 2007 IOP Publishing Ltd Printed in the UK

theoretical efforts have been focused on the synthesizing and designing the new superhard materials with hardness comparable to that of diamond [1–5]. Recently, Cumberland *et al* demonstrated that hardness may be increased by introducing a small, covalent bond-forming atom such as boron, carbon, nitrogen and oxygen into a transition metal with a high bulk modulus but low hardness [3–5]. As an example, they reported the synthesis, bulk modulus, and preliminary hardness testing of osmium diborides, OsB_2. The results indicated that OsB_2 was a low compressible and hard compound, with the bulk modulus in the range of 365–395 GPa and the compressibility along the c-direction even less than that of diamond [5]. OsB_2 has an orthorhombic lattice (space group $Pmmn$, No. 59) with the experimental lattice parameters $a = 4.684$ Å, $b = 2.872$ Å, and $c = 4.076$ Å [6]. In the orthorhombic structure, two Os atoms occupy the 2a Wyckoff sites and four B atoms hold the 4f sites. Because no adequately sized single crystal might be obtained, the theoretical calculations based on the density functional theory were employed to provide crucial information for the understanding of the physical properties, and suggested that the high hardness is the result of the covalent bonding between osmium d states and boron p states [7–10]. Furthermore, it is known that hardness might be enhanced when two dissimilar phases are intermixed, since the mixed metals can act as barriers to the movement of dislocations [4]. Hence, it is possible that the bulk modulus and hardness of OsB_2 can be exceeded by doping with other transition metals such as ruthenium, iridium and rhenium [3–5].

However, most of the interest on this kind of possible hard materials has been so far limited to OsB_2 [7–10], available extended and systematic study of TMB_2 (TM = Hf, Ta, W, and Re, Os, Ir and Pt) in the $Pmmn$ space group is lacking at present, which may help the comprehension of the physical mechanisms determining the elastic properties and possibly guide the discovery of even more promising compounds. Moreover, it is necessary to give clear suggestions of how to exceed the bulk modulus and hardness of OsB_2 through transition metals doping. This paper, therefore, focuses on the extension of first-principles calculations to the entire 5d transition metals series diborides in the orthorhombic structure, and on studies in detail the heat of formation, cohesive energy as well as its corresponding structural, electronic and elastic properties. Furthermore, we observe that there are trends in elastic constant as a function of the valence electron concentration (VEC $= \frac{(n_{TM}+2n_B)}{3}$, where n_{TM} and n_B denote the number of valence electron for transition metal and boron, respectively). According to the observed trends, we predict alloying W and Re in the orthorhombic structure OsB_2 might be harder than combination with Ir element. In order to validate this predication, we work with three compounds obtained by modifying OsB_2 in the supercell: $Os_{0.5}TM_{0.5}B_2$ (TM = W, Re and Ir).

2. Theoretical method

The calculations were performed here based on the total energy code CASTEP, in which a plane-wave pseudopotential total energy calculation was utilized [11]. Within the first-principles calculations, interactions of electrons with ion cores were represented by the Vanderbilt-type ultrasoft pseudopotential [12]. The exchange correlation functional was treated under the generalized gradient approximation (GGA) as proposed by Perdew, Burke and Ernzerhof (PBE) [13]. The plane-wave basis set cut-off was set as 400 eV for all cases. The special points sampling integration over the Brillouin zone was employed by using the Monkhorst–Pack method with a grid of 0.04 $Å^{-1}$ [14]. Convergence of the total energy with a different number of k points and the plane-wave cut-off energy has been tested. The Broyden–Fletcher–Goldfarb–Shanno (BFGS) minimization scheme [15] was used in geometry

optimization. The tolerances for geometry optimization were set as the difference in total energy being within 5×10^{-6} eV/atom, the maximum ionic Hellmann–Feynman force within 0.01 eV Å^{-1}, the maximum ionic displacement within 5×10^{-4} Å and the maximum stress within 0.02 GPa.

The elastic constants were determined by applying a set of given homogeneous deformation with a finite value and calculating the resulting stress with respect to optimizing the internal atomic freedoms, as implemented by Milman *et al* [16]. The criteria for convergence of optimization on atomic internal freedoms were selected as differences in the total energy within 1×10^{-6} eV/atom, ionic Hellmann–Feynman forces within 0.002 eV Å^{-1}, and the maximum ionic displacement within 1×10^{-4} Å. Three strain patterns brought out stresses related to all the nine independent elastic coefficients for the orthorhombic unit cell. Three positive and three negative amplitudes were applied for each strain component with a maximum strain value of 0.3%. The compliance matrix S was calculated as the inverse of the stiffness matrix, $S = C^{-1}$. All the calculations performed here were in absence of spin-polarized and the spin–orbit coupling.

3. Results and discussions

3.1. Structure, heat of formation, cohesive energy and elastic properties of the pure phases

To compute the equilibrium crystal structure of 5d transition metal diborides, we optimized the previously reported [6] crystal structure of OsB_2 by relaxing the cell degrees of freedom with constrained space group $Pmmn$. The calculated lattice parameters and unit cell volumes for the 5d transition metal diborides are shown in table 1, along with the available experimental and theoretical data for comparison. The theoretical lattice constants of OsB_2 obtained from the GGA method is in good agreement with the experimental values [6] and the previous theoretical values [7–10]. The calculated density of OsB_2 is 13.0071 g cm^{-3} and agrees well with the experimental value 12.8295 g cm^{-3} [6] and the previous theoretical values 13.196 at LDA level and 12.907 g cm^{-3} [7] at GGA level. Therefore, the present first-principles calculation is able to reliably reproduce the equilibrium crystal structure of OsB_2. For the other 5d transition metal diborides in the hypothetical structure, there are no available experimental lattice parameters; however, taking account of the cases of OsB_2, we believe our predicted values should be reliable. Furthermore, it should be noted that the bond lengths of TM–B are consistent with those of experimentally observed structures. For example, the range of bond length of the Hf–B is 2.383–2.568 Å in this calculation. This is in agreement with the experimental value in the $P6/mmm$ space group, 2.510 Å [17].

In order to check the probability of the existence of the 5d transition metal diborides in the $Pmmn$ space group, we calculated the heat of formation ΔH^{TMB_2} from the total energy of the crystal $E^{TMB_2}_{total}$ as well as the pure elemental constituents E^{TM}_{solid}, E^{B}_{solid} as follows:

$$\Delta H^{TMB_2} = E^{TMB_2}_{total} - [E^{TM}_{solid} + 2E^{B}_{solid}]$$

E^{TM}_{solid} was calculated in the pure metal lattices. Simultaneously, the most stable allotrope of crystalline boron (α-B_{12}) is used. The implication of this definition is that if ΔH^{TMB_2} is negative, the transition metal diboride can form, while if it is positive, the compound is thermodynamic unstable to a separation into the elemental metal and B.

In this study, the theoretical heat of formation for the series of the TM–B group are listed in table 1 and illustrated in figure 1(a). It is seen that the heat of formation of OsB_2 is -0.121 eV/atom. This result corresponds to the experiment that this phase is stable under the ambient conditions. The computed heat of formation yields $+1.616$ eV/atom for HfB_2,

Table 1. Calculated equilibrium lattice parameters (Å) and equilibrium volume (Å^3/cell), density (g cm^{-3}) of the TMB_2 (TM = Hf–Pt) and compared with available experimental data, as well as the cohesive energy (eV/atom), and heat of formation (eV/atom).

Compound	a	b	c	ρ	E_{coh}	ΔH	Volume
HfB_2	5.031	3.057	4.549	9.50001	7.099	1.616	34.9779
TaB_2	4.751	2.954	4.279	11.2032	7.527	−0.185	30.0247
WB_2	4.647	2.944	4.205	11.8601	8.185	−0.177	28.7681
ReB_2	4.578	2.869	4.078	12.8815	8.889	−0.204	26.7907
OsB_2	4.652	2.859	4.066	13.0071	8.457	−0.121	27.0417
OsB_2[a]	4.684	2.872	4.076	12.8295			27.4161
OsB_2[b]	4.6365	2.8427	4.0445	13.196			26.6554
OsB_2[c]	4.6645	2.8679	4.0743	12.907			27.2516
OsB_2[d]	4.6444	2.8505	4.0464				26.89
OsB_2[e]	4.7049	2.8946	4.0955				27.99
OsB_2[f]	4.6433	2.8467	4.0432				26.72
OsB_2[g]	4.6383	2.8437	4.0388				26.635
OsB_2[h]	4.648	2.846	4.047				26.823
IrB_2	4.486	3.136	3.971	12.7115	7.877	−0.111	27.9346
PtB_2	4.777	3.057	4.045	12.1845	6.429	0.077	29.5338

[a] Reference [5], experimental study.
[b] Reference [7], theoretical study at local density approximation (LDA) level.
[c] Reference [7], theoretical study at generalized gradient approximation (GGA) level.
[d] Reference [8], theoretical study at LDA level.
[e] Reference [8], theoretical study at GGA level.
[f] Reference [9], theoretical study at local spin density approximation (LSDA) level.
[g] Reference [9], theoretical study at LSDA + SO (SO indicates spin–orbit coupling) level.
[h] Reference [10], theoretical study at LDA level.

−0.185 eV/atom for TaB_2, −0.177 eV/atom for WB_2, −0.204 eV/atom for ReB_2, and −0.111 eV/atom for IrB_2, +0.074 eV/atom for PtB_2, respectively. These results suggest the thermodynamic stability of these compounds except HfB_2 and PtB_2. Among the TMB_2 compounds, some hexagonal phases [18–20] have been synthesized and characterized in experiments. Thus, the compounds within *Pmmn* space group remain metastable for TM = Ta, W, Re and Ir with negative heat of formation, indicating these materials might be easily synthesized experimentally.

It is also noteworthy that the cohesive energy of a material is another fundamental property which is a measure of the strength of the forces that bind atoms together in the solid state and is descriptive in studying the phase stability. The cohesive energy $E_{coh}^{TMB_2}$ of TMB_2 is defined as the total energy of the constituent atoms minus the total energy of the compound

$$E_{coh}^{TMB_2} = [E_{atom}^{TM} + 2E_{atom}^{B}] - E_{total}^{TMB_2},$$

where $E_{total}^{TMB_2}$ refers to the total energy of TMB_2 in the equilibrium configuration and E_{atom}^{TM}, E_{atom}^{B} are the pseudo-atomic energies of transition metal and boron, respectively. The computed values of cohesive energies of all considered compounds are also given in table 1 and illustrated in figure 1(b). It shows that the cohesive energies of the 5d transition metal diborides increase monotonously up to Re, then decrease. This trend can be understood in terms of the band filling principle [21], see below. Generally speaking, the cohesive energy that is a measure of the strength of the forces binding atoms together in the solid state, is expected to change in the same trend as the bulk modulus which represents the resistance to volume change and is related to the overall atomic binding properties in a material [22]. Therefore, ReB_2 is expected to have the highest bulk modulus and this is indeed confirmed later.

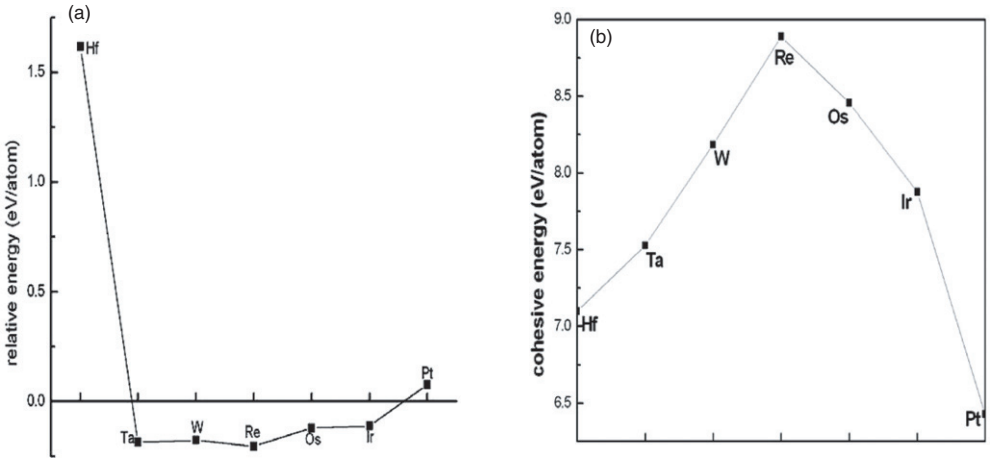

Figure 1. (a) The heat of formation for transition metal diborides considered in the present study, versus the position of the transition metal in the periodic table. The line is a guide for the eye. (b) The cohesive energy for transition metal diborides considered in the present study, versus the position of the transition metal in the periodic table. The line is a guide for the eye.

Since these thermodynamic stable compounds except OsB_2 have not been observed in experiment within the *Pmmn* space group, it is necessary to explore the mechanical stability for these compounds. The mechanical stability of a crystal, which means that the strain energy must be positive, is checked by the whole set of elastic constants C_{ij} which satisfies special restrictions. The requirements of elastic stability for an orthorhombic crystal, which has nine independent elastic constants, are as follows [23, 24]:

$$C_{11} > 0, \quad C_{22} > 0, \quad C_{33} > 0, \quad C_{44} > 0, \quad C_{55} > 0, \quad C_{66} > 0,$$
$$(C_{11} + C_{22} - 2C_{12}) > 0, \quad (C_{11} + C_{33} - 2C_{13}) > 0, \quad (C_{22} + C_{33} - 2C_{23}) > 0,$$
$$(C_{11} + C_{22} + C_{33} + 2C_{12} + 2C_{13} + 2C_{23}) > 0.$$

The calculated elastic constants are given in table 2. Our calculated elastic constants for OsB_2 are consistent with those previous results [7, 8] with about 20–40 GPa deviation. We attribute this discrepancy to the difference in the lattice parameters used in the calculations. In addition, one should be aware that the values presented in table 2 were obtained at $T = 0$ K, and that temperature effects generally reduce the elastic constants. Therefore, we expect the experimental values at room temperature to be smaller than those presented here. The results suggested that the HfB_2 and PtB_2 in the *Pmmn* space group to be either unstable or extremely soft, while TaB_2, WB_2, ReB_2 and IrB_2 are mechanically stable phases under the ambient conditions.

The accurate calculation of elasticity is essential for understanding the macroscopic mechanical properties of solids and for the design of hard materials. Elasticity describes the response of a crystal under external strain and provides key information of the strength of the material, as characterized by bulk modulus, shear modulus, Young's modulus, and Poisson's ratio [23]. These parameters can be calculated from the single-crystal zero-pressure elastic constants, using the Voigt–Reuss–Hill approximation [25], as presented in table 3.

The obtained bulk modulus of OsB_2 317 GPa, is smaller than the experimental value of 365–395 GPa [5]. The underestimation of bulk modulus is typical for GGA calculations. Our calculations reproduced isotropic bulk modulus, shear modulus, Young's modulus and Poisson's ratio for polycrystalline aggregate OsB_2 very well in comparison with the previous

Table 2. Calculated zero-pressure elastic constant c_{ij} (GPa) of the TMB_2 (TM = Hf–Pt).

	C_{11}	C_{22}	C_{33}	C_{44}	C_{55}	C_{66}	C_{12}	C_{13}	C_{23}
HfB_2	364	237	417	−16	127	113	96	95	151
TaB_2	468	467	744	45	241	218	185	138	91
WB_2	496	532	857	184	292	217	221	160	82
ReB_2	595	595	935	214	332	276	212	178	109
OsB_2	570	568	786	78	220	212	174	189	118
OsB_2[a]	585	588	827	61	225	217	180	195	124
OsB_2[b]	546	553	763	64	209	207	166	184	113
OsB_2[c]	597.0	581.2	825.0	70.1	212.0	201.3	198.1	206.1	142.6
IrB_2	453	397	747	73	24	151	259	186	170
PtB_2	385	282	567	−27	−85	90	196	228	153

[a] Reference [7], theoretical study at LDA level.
[b] Reference [7], theoretical study at GGA level.
[c] Reference [8], theoretical study at LDA level.

Table 3. The isotropic bulk modulus B_H (GPa), shear modulus G_H (GPa), Young's modulus E_H (GPa) and Poisson's ratio ν_H for polycrystalline aggregate TMB_2 (TM = Hf–Pt) from the single-crystal elastic constants by means of Reuss's, Voigt's and Hill's approximations.

	B_V	B_R	$B_H = (B_V + B_R)/2$	G_V	G_R	$G_H = (G_V + G_R)/2$	G_H/B_H	E_H	ν_H
HfB_2	189	179	184						
TaB_2	278	273	276	185	120	153	0.55	387	0.2660
WB_2	312	306	309	248	212	230	0.74	553	0.2018
ReB_2	347	339	343	272	256	264	0.77	630	0.1937
OsB_2	320	315	317	198	162	180	0.57	454	0.2612
OsB_2[a]			365–395						
OsB_2[b]			332			174	0.546	444	0.277
OsB_2[c]			307			168	0.523	426	0.269
OsB_2[d]			336.1						
OsB_2[e]			303.45						
OsB_2[f]			364.7						
OsB_2[g]			385.4						
OsB_2[h]			364.87						
IrB_2	311	304	307	115	68	92	0.30	251	0.3638
PtB_2	265	241	253						

[a] Reference [6], experimental study.
[b] Reference [7], theoretical study at LDA level.
[c] Reference [7], theoretical study at GGA level.
[d] Reference [8], theoretical study at LDA level.
[e] Reference [8], theoretical study at GGA level.
[f] Reference [9], theoretical study at LSDA level.
[g] Reference [9], theoretical study at LSDA + SO level.
[h] Reference [10], theoretical study at LDA level.

theoretical study [7]. However, we also noticed that the calculated bulk modulus (317 GPa) of OsB_2 is smaller than that (462 GPa [26], 411 GPa [27]) of the parent metal: osmium. Although it is expected that OsB_2 should have larger bulk modulus than their parent metal due to the directional bonding introduced by the boron atoms in the lattice, Grossman *et al* have shown that the addition of small, covalent bond-forming atoms such as boron, carbon and nitrogen should not increase its hardness, due to the fact that the late (heavier) transition metals have a more corrugated density distribution in their elemental phases, such as W and Os [28].

Table 4. Longitudinal, transverse, average sound velocity (υ_t, υ_l and υ_m in km s^{-1}) and the Debye temperature θ_D (K) obtained from the average sound velocity with GGA calculation.

	υ_t	υ_l	υ_m	θ_D
TaB_2	3.69	6.54	4.10	566
WB_2	4.40	7.20	4.86	681
ReB_2	4.53	7.34	4.99	716
OsB_2	3.72	6.54	4.13	591
IrB_2	2.69	5.81	3.03	428

On the basis of the previous discussion on the cohesive energy, one might suspect that the bulk modulus for the series of the TM–B group should take the same trend compared to the cohesive energies. Indeed, this is true except for HfB_2 and PtB_2 (tables 1 and 3). We believe that the root of the discrepancy is associated with the thermodynamic and mechanical unstable properties of these two compounds. Moreover, there is an obvious relationship between the bulk modulus and the unit cell volumes: the softest material (i.e., with the lowest bulk modulus) has the largest unit cell volume. Surprisingly, the high G/B ratio or, equivalently, the low Poisson's ratio (ν) of WB_2 and ReB_2 point to a high degree of covalency, suggesting that intercalation of the boron into transition metal lattices induces a substantial change of the electronic structure from metallic to covalent in WB_2 and ReB_2.

In addition, from the zero-temperature elastic constants we can obtain some information on the thermal properties for the series of the TM–B group. The transverse and longitudinal acoustic velocities can be calculated as follows:

$$\upsilon_t = \sqrt{\frac{G_h}{\rho}},$$

$$\upsilon_l = \sqrt{\left(B_h + \tfrac{4}{3}G_h\right)/\rho}.$$

Here ρ is the mass density of the material. We can then define the mean sound velocity as

$$\frac{1}{\upsilon_m^3} = \frac{1}{3}\left(\frac{1}{\upsilon_t^3} + \frac{2}{\upsilon_l^3}\right).$$

For a solid with N_0 atoms in the volume V, the Debye temperature θ_D may be estimated from the mean sound velocity by the equation

$$\theta_D = (h\upsilon_m/k_B)(3N_0/4\pi V)^{1/3},$$

where h is Plank's constant and k_B is the Boltzmann constant [23]. The computed longitudinal, transverse, average sound velocity and the Debye temperature obtained from the average sound velocity with GGA calculation are shown in table 4. For ReB_2, the largest B and G values result in the largest sound velocity and Debye temperature compared to the other compounds. Although the experimental values of the Debye temperature and sound velocity are not yet available, considering the above calculated results, we believe that our predicted values should be reliable. It should be pointed out that the Debye temperature induced from the elastic constants should be consistent with the value determined from specific heat measurements at low temperatures, due to the main contribution of the acoustic vibrations [29].

3.2. Trends in elastic stiffness with respect to VEC for the series of transition metal diborides

In light of these results, we classified the elastic properties of these materials according to their valence electrons concentration VEC, shown in figures 2–4. The curve is obtained by quadratic

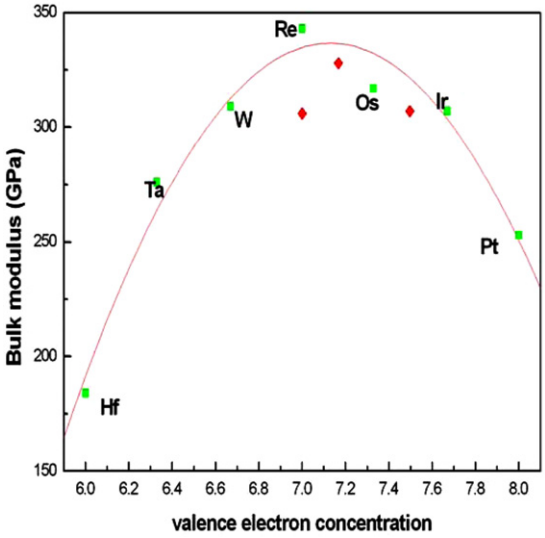

Figure 2. The theoretical bulk modulus B (the square) of TMB_2 (TM = Hf–Pt) with respect to number of valence electrons per atom (VEC). The solid curve is obtained by quadratic fitting to bulk modulus of TMB_2 at each VEC. The bulk modulus B (the diamond) of $Os_{0.5}TM_{0.5}B_2$ (TM = W, Re, and Ir) are also presented.

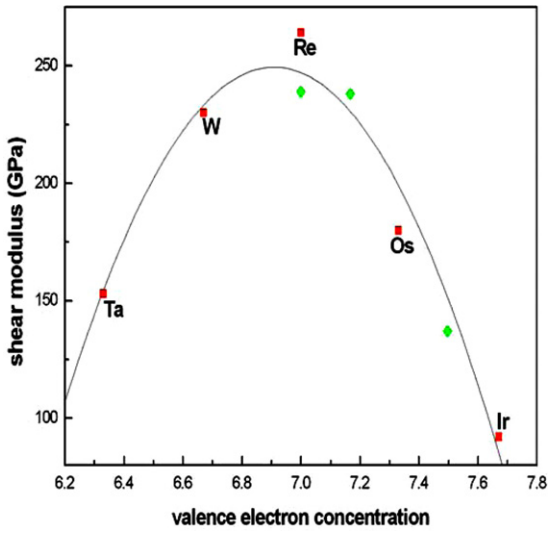

Figure 3. The calculated shear moduli G (the square) of TMB_2 (TM = Ta–Ir) with respect to valence electron concentration (VEC). The solid curve is obtained by quadratic fitting to shear moduli of TMB_2 at each VEC. The shear modulus B (the diamond) of $Os_{0.5}TM_{0.5}B_2$ (TM = W, Re, and Ir) are also presented.

fitting to the calculated bulk modulus and shear modulus, respectively. The deviation from the fitted data is within 20 GPa for bulk and shear modulus of all compounds considered in the present work, which is in the range of the error of the calculated bulk modulus and shear

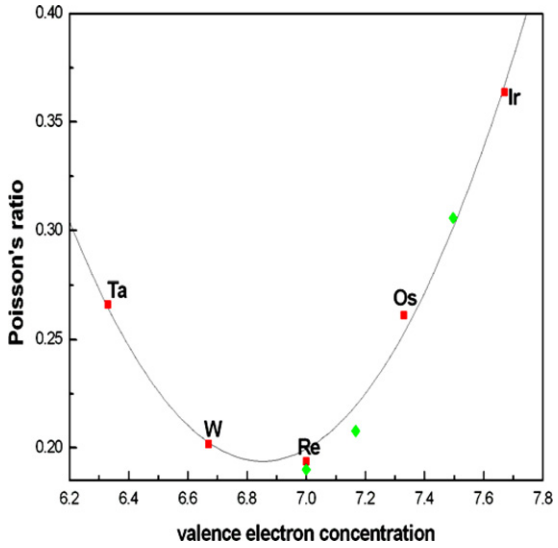

Figure 4. The Poisson's ratio ν (the square) of TMB_2 (TM = Ta–Ir) with respect to valence electron concentration (VEC). The solid curve is obtained by quadratic fitting to Poisson's ratio of TMB_2 at each VEC. The Poisson's ratio ν (the diamond) of $Os_{0.5}TM_{0.5}B_2$ (TM = W, Re, and Ir) are also presented.

modulus, 15–30 GPa.[5] The most interesting feature is that there is a clear dependence of bulk modulus, shear modulus and Poisson's ratio on VEC. The calculated bulk modulus and shear modulus reach the maximum at VEC range of 6.8–7.2, and while the Poisson's ratio reaches the minimum.

To understand this behaviour of elastic properties on a fundamental level, we examined the characteristics of electronic structure for the studied compounds. The band structures of TMB_2 (TM = Hf, Ta, W, Re, Os, Ir and Pt) are presented in figure 5. It is seen that the Fermi level systematically shifts upwards from HfB_2 to PtB_2 due to the increase of valence electrons. Further, all these compounds possess finite $N(E_F)$ at the Fermi level, indicating metallic behaviour.

The density of states (DOS) of TMB_2 is shown in figure 6 where the vertical line indicates Fermi level. The DOS curves mainly consist of three parts: (1) the peak in the low energy interval (from −15 to −10 eV) is mainly due to the localized or tightly bound 2s electrons of B; (2) the bonding states of TM 5d and B 2p orbitals are near the Fermi level, and (3) the DOS curve above the Fermi level is due to antibonding states. It is also seen that the DOS of TM 5d and B 2p are energetically degenerate, indicating the covalent hybridization between TM and B atoms. In addition, the electrons from TM 5d and B 2p states both contribute to the density of states at the Fermi level. The typical feature of the total DOS of these compounds is the presence of a pseudogap which has also been observed in many early transition metal diborides and is considered as an indicator of the boundary between the bonding states and antibonding states [30]. The appearing of pseudogap is believed to originate mainly from B–B covalent hybridization, while TM–TM or TM–B covalent interactions are less significant to the creation of the pseudogap [30].

[5] We estimate the numerical error on the elastic constant C_{ii} (i = 1–6) to be of the order of 5–10% while the elastic constants C_{12}, C_{13} and C_{23} are expected to have larger numerical errors since the corresponding polynomial fits also incorporating the calculated values of C_{11}, C_{22} and C_{33}. Thus the numerical error of the calculated bulk modulus and shear modulus should be in the range of 15–30 GPa at least.

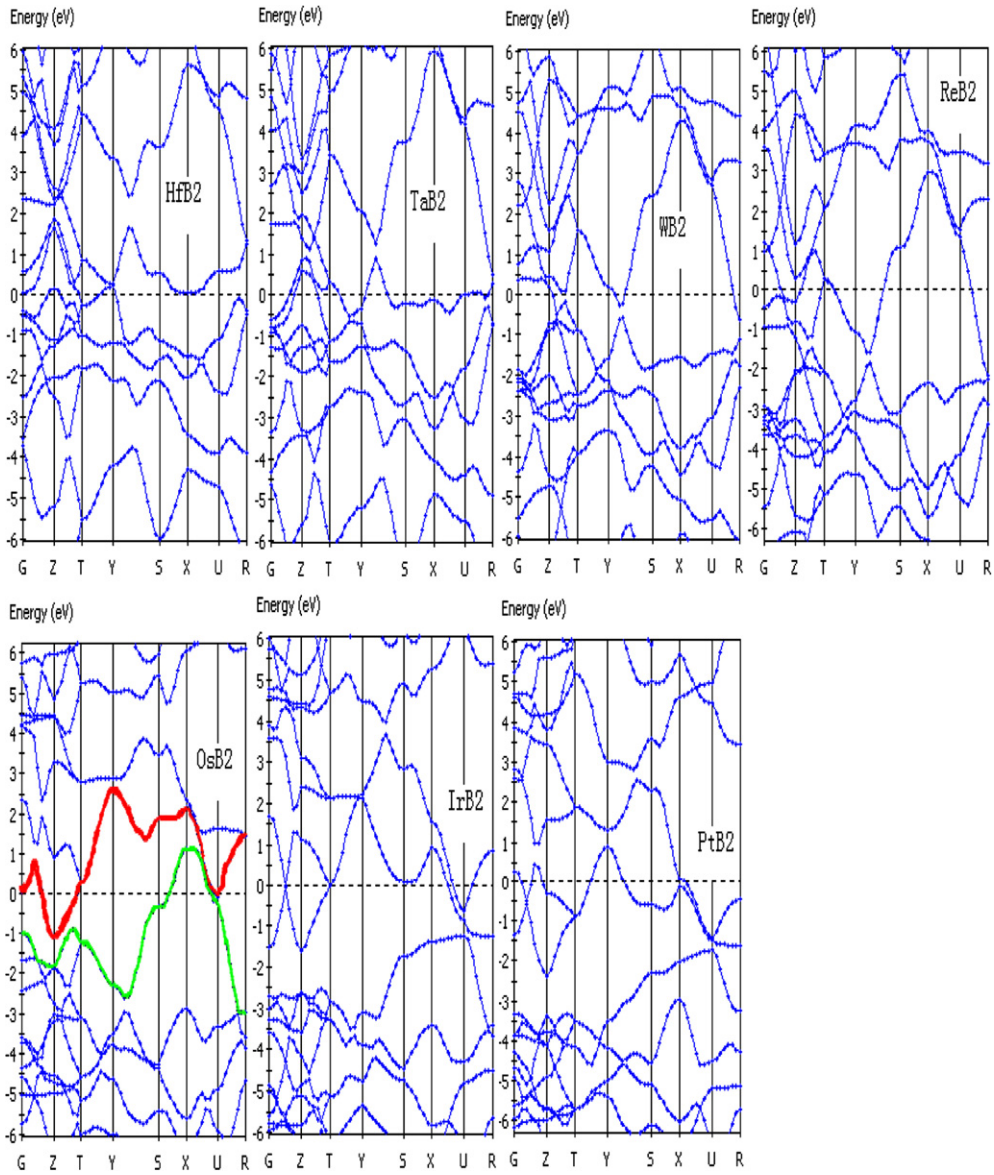

Figure 5. The electronic band structures of the transition metal diborides studied at high symmetry points calculated using the generalized gradient approximation (GGA) with Fermi energy level taken at 0 eV as shown by the dotted line in the *Pmmn* space group. In the OsB_2 picture, the green line (the lower fat line which just crosses the Fermi energy level) represents the highest occupied p–d bonding state, while the red line (the higher fat line which just crosses the Fermi energy level) stands for the lowest unoccupied antibonding state.

The trends in bulk modulus, shear modulus and Poisson's ratio as VEC can be understood in terms of chemical bonding due to the different occupation of valence electrons for the studied compounds. Compared with HfB_2, in TaB_2, the additional valence electron continues to fill the p–d bonding states. This results in the increase of the cohesive energy and leads to enhanced bulk modulus and shear modulus. Whereas for WB_2, ReB_2 and OsB_2, the Fermi level is localized at pseudogap that splits the occupied bonding states and unoccupied antibonding

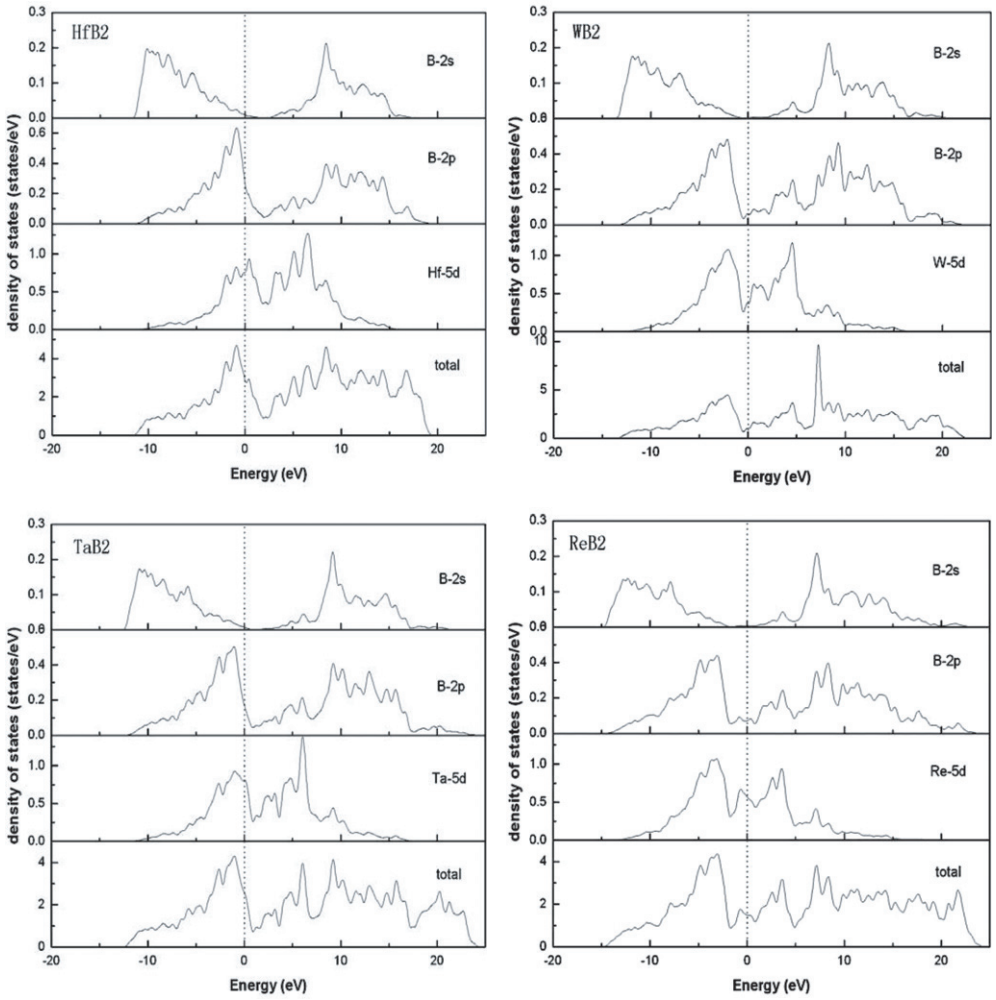

Figure 6. Total and partial density of states for selected transition metal diborides. The dotted line at zero is the Fermi energy level.

states, indicating the p–d bonding states tend to be filled completely. Therefore, these three compounds have large cohesive energies, and large bulk modulus and shear modulus, while the Poisson's ratio is small. It should be pointed out that the antibonding states begin to fill in OsB_2 (figure 6). On the other hand, for IrB_2 and PtB_2, the excessive occupation of the p–d antibonding states gives rise to a negative contribution to the bonding energy and the elastic shear resistance, i.e., decreases the cohesive energy, bulk modulus and shear modulus significantly. Note that the equilibrium volume reaches the minimum when the bonding states are completely filled and beyond this, it increases with the filling of antibonding states. This trend can be seen from the equilibrium volume given in table 1.

Based on these discussions, for the compound at the beginning of this series, the bonding states start to fill, leading to increase in cohesive energy and a decrease in the atomic volume. This decreased atomic volume and increased cohesive energy result in an increase in bulk modulus, shear modulus and decrease in Poisson's ratio. These effects are all maximized near the middle of the transition series, when all the bonding states are filled. And then, this trend

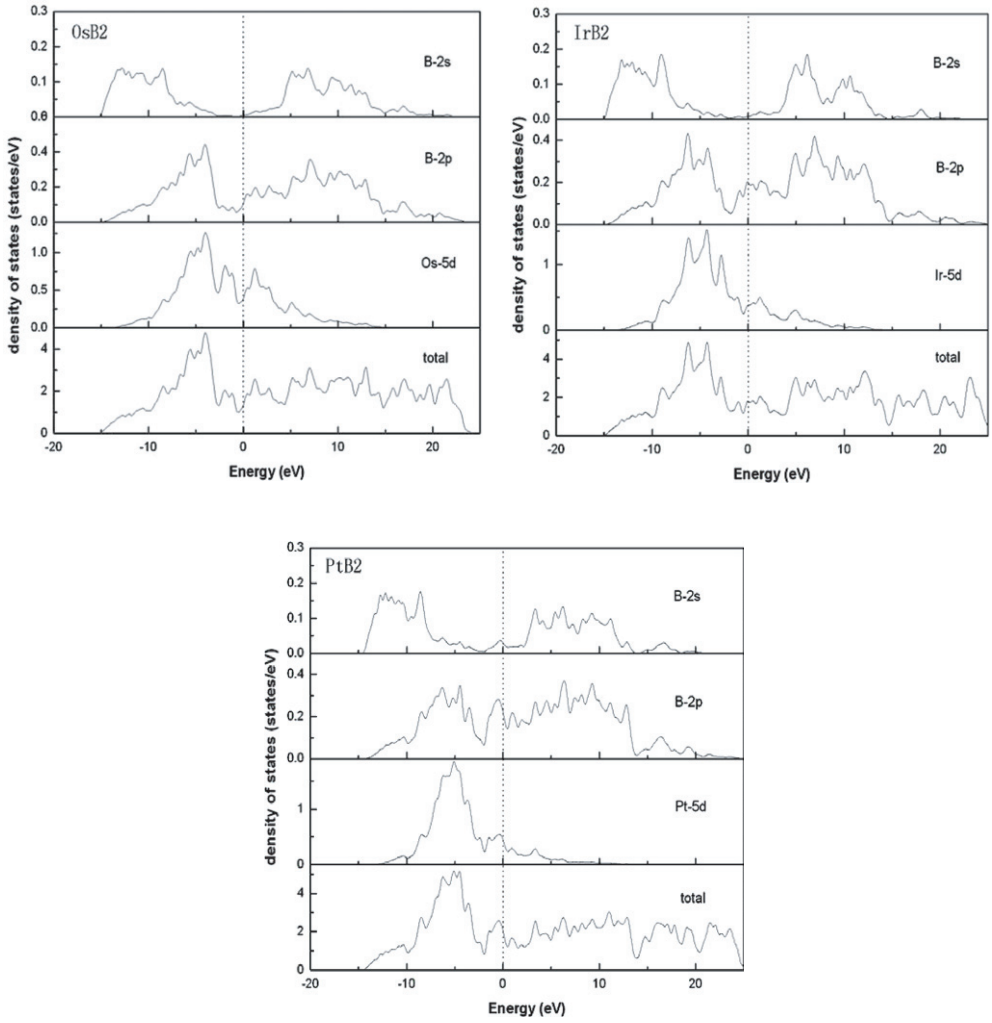

Figure 6. (Continued.)

is reversed when the antibonding states begin to be filled. These interpretations are consistent with our calculations of the trend of the cohesive energy, which are given in figure 1(b) and table 1, and in agreement to the calculated bulk modulus, shear modulus and Poisson's ratio (see figures 2–4, and table 3).

More importantly, We note that the peak of the fitted curves in figures 2–4 is roughly at the range of 6.8–7.2, corresponds to nearly full occupation of the highest bonding state without filling the lowest antibonding state. This result strongly suggests that while OsB_2 is hard, the doping of other transition metal element(s) in OsB_2 might achieve larger bulk modulus and shear modulus by tuning the VEC to an optimum value. In addition, one of the three conditions must be met in order for a material to be hard, is that the material must not deform plastically and the creation and motion of the dislocations must be as small as possible [31]. Indeed, it is well known that mixed metals can act as barriers to the movement of dislocations, and thus mixed-metal borides could be expected to be harder [3–5]. According to this point, alloying W or Re in this orthorhombic structure OsB_2 might be harder than combination with Ir element.

Table 5. The calculated equilibrium lattice parameters (Å), volume V (Å^3/cell), heat of formation ΔH (eV/atom) and zero-pressure elastic constant c_{ij} (GPa), and isotropic bulk modulus B_H (GPa), shear modulus G_H (GPa), Young's modulus E_H (GPa) and Poisson's ratio ν_H for polycrystalline aggregate $Os_{0.5}TM_{0.5}B_2$ (TM = W, Re and Ir) from the single-crystal elastic constants using Reuss's, Voigt's and Hill's approximations.

	$Os_{0.5}W_{0.5}B_2$	$Os_{0.5}Re_{0.5}B_2$	$Os_{0.5}Ir_{0.5}B_2$
a	4.6590	4.6019	4.6180
b	2.9222	2.8752	2.9548
c	4.1231	4.0624	4.0208
V	28.0670	26.8754	27.4328
ΔH	0.074	−0.164	−0.104
C_{11}	564	625	496
C_{22}	542	597	407
C_{33}	841	873	741
C_{44}	190	169	104
C_{55}	265	283	98
C_{66}	231	222	185
C_{12}	171	151	252
C_{13}	150	178	182
C_{23}	98	121	149
B_V	302	324	302
B_R	309	332	312
B_H	306	328	307
G_V	249	244	148
G_R	229	233	127
G_H	239	238	137
E_H	569	577	358
ν_H	0.1901	0.2078	0.3058

3.3. The structural and elastic properties of $Os_{0.5}TM_{0.5}B_2$ (TM = W, Re and Ir)

In order to validate our predication stated above, the transition metal substitution calculations using supercell approximation were performed. For simplicity, we have worked with a unit cell which contained 50% substitution. While the concentrations of transition metals substitution have been taken to be rather high to keep computational costs low, it is expected to give insight into our prediction. The calculated lattice parameters, the relative heat of formation and zero-pressure elastic constant c_{ij} are summarized in table 5, along with the induced isotropic bulk modulus B_H, shear modulus G_H, Young's modulus E_H and Poisson's ratio ν_H for polycrystalline aggregate from the single-crystal elastic constants using Reuss's, Voigt's and Hill's approximations. And the corresponding points (the diamond) are also shown in figures 2–4.

It is usually assumed that hardness is defined by the elastic moduli: bulk modulus, a measure of resistance to volume change by applied pressure, and shear modulus, a measure of resistance to reversible deformations upon shear stress [32]. Generally, the search for hard materials is simplified to search materials with large bulk modulus or shear modulus, because there is a direct relation between bulk modulus, shear modulus and hardness [33]. The calculated bulk modulus and the shear modulus for $Os_{0.5}Re_{0.5}B_2$ are 328 and 238 GPa, which is higher than the corresponding values of OsB_2 (317 and 180 GPa). This is a strong indication that the solid solution $Os_{0.5}Re_{0.5}B_2$ may be harder than the compound OsB_2, hence making it desirable to be a low compressibility and hard material. Similarly, $Os_{0.5}W_{0.5}B_2$ can also be considered as a hard material. In addition, Jhi *et al* [33] demonstrated that the magnitude of

the shear modulus C_{44}, rather than the bulk modulus B and shear modulus G, was a better hardness predictor for transition metal carbonitrides. If this were true for the present studied compounds, the high values of C_{44} for $Os_{0.5}Re_{0.5}B_2$ (169 GPa) and $Os_{0.5}W_{0.5}B_2$ (190 GPa), compared to OsB_2 (78 GPa), might also suggest that $Os_{0.5}Re_{0.5}B_2$ and $Os_{0.5}W_{0.5}B_2$ are harder than OsB_2. On the other hand, the relative small shear modulus (137 GPa) and large Poisson's ratio (0.3058) of $Os_{0.5}Ir_{0.5}B_2$, indicate that combination with the elements on the right side of Os of 5d group (such as Ir) may soften the hardness of OsB_2. Here it is worth noting that although the elastic properties are regarded as a measure of hardness of materials, it is not always positively correlated with the experimentally measured hardness, and the existence of a degree of metallic character will reduce the shear strength, as proved by the compound: tungsten carbide [31].

In order to decide whether the doping OsB_2 is possible, we calculated the heat of formation energy for these defect structures. From table 5, the negative values for $Os_{0.5}Re_{0.5}B_2$ and $Os_{0.5}Ir_{0.5}B_2$ indicate that they might be formed, while the small positive one for $Os_{0.5}W_{0.5}B_2$ suggests it is thermodynamic unstable and could not be formed under the ambient conditions. However, special synthesized methods may overcome such small positive value and achieve this interesting solid solution, such as under high pressure/high temperature conditions.

Finally, the computed bulk modulus, shear modulus and Poisson's ratio of these three solid solutions, are reasonably consistent with the trends in the elastic stiffness with respect to valence electron concentration (figures 2–4). This picture indicates that tuning VEC is an effective method to optimize the desired elastic properties in this solid solution. In a word, our calculations consolidate the above-mentioned predication, and indicate that solid solution hardening might be operative in $Os_{1-x}TM_xB_2$ alloys within a certain VEC range, that is, tailoring the system's elastic properties could be done by tuning the valence electron concentration.

4. Concluding remarks

In summary, we calculate the cohesive energy, the elastic properties and discussed the relationship between elastic stiffness and valence electron concentration of TMB_2 in the $Pmmn$ space group, where TM stands for Hf, Ta, W, Re, Os, and Ir, Pt. The theoretical trends are well interpreted in terms of bonding characteristics of states near the Fermi level. The results indicate that the maximum in bulk modulus, shear modulus and minimum in Poisson's ratio originate from the nearly complete filling the p–d bonding states without filling the p–d antibonding states between the transition metal and boron atoms. The bulk modulus and shear modulus reach their maximum as the VEC is the range of 6.8–7.2, while the Poisson's ratio reaches the minimum. Such noninteger VEC can be achieved by alloying such as $Os_xRe_{1-x}B_2$. On the basis of the theoretical trends, alloying W or Re in this orthorhombic structure OsB_2 is predicted to be harder than combination with Ir element. Indeed, we consolidate the predication through the transition metal substitution calculations using supercell approximation. More importantly, we find a clue to tailor the desired elastic properties by properly tuning its valence electron concentration of $Os_{1-x}TM_xB_2$ solid solution.

Acknowledgments

We sincerely thank the reviewers for valuable suggestions. The work was financially supported by the National Natural Science Foundation of China (Grant Nos 20331030, 20571073, 20661026 and 20671088). X F Hao thanks Yanshan University for computer time.

References

[1] Solozhenko V L, Andrault D, Fiquet G, Mezouar M and Rubie D C 2001 *Appl. Phys. Lett.* **78** 1385
[2] Thornton A G and Wilks J 1978 *Nature* **274** 792
[3] Gilman J J, Cumberland R W and Kaner R B 2006 *Int. J. Refract. Met. Hard Mater.* **24** 1
[4] Kaner R B, Gilman J J and Tolbert S H 2005 *Science* **308** 58
[5] Cumberland R W, Weinberger M B, Gilman J J, Clark S M, Tolbert S H and Kaner R B 2005 *J. Am. Chem. Soc.* **127** 7264
[6] Aronsson B 1963 *Acta Chem. Scand.* **17** 2036
[7] Gou H Y, Hou L, Zhang J W, Li H, Sun G F and Gao F M 2006 *Appl. Phys. Lett.* **88** 221904
[8] Hou Z F 2006 *Phys. Rev.* B **74** 012102
[9] Chen Z Y, Xiang H J, Yang J L, Hou J G and Zhu Q S 2005 *Preprint* cond-mat/0508506 (unpublished)
[10] Chiodo S, Gotsis H J, Russo N and Sicilia E 2006 *Chem. Phys. Lett.* **425** 311
[11] Segall M D, Lindan P J D, Probert M J, Pickard C J, Hasnip P J, Clark S J and Payne M C 2002 *J. Phys.: Condens. Matter* **14** 2717
[12] Vanderbilt D 1990 *Phys. Rev.* B **41** 7892
[13] Perdew J P, Burke K and Ernzerhof M 1996 *Phys. Rev. Lett.* **77** 3865
[14] Monkhorst H J and Pack J D 1977 *Phys. Rev.* B **16** 1748
[15] Pfrommer B G, Côté M, Louie S G and Cohen M L 1977 *J. Comp. Physiol.* **131** 233
[16] Milman V and Warren M C 2001 *J. Phys.: Condens. Matter* **13** 241
[17] Cannon J F and Fransworth P B 1983 *J. Less-Common Met.* **92** 359
[18] Lönnberg B 1988 *J. Less-Common Met.* **141** 145
[19] Woods H P, Wawner F E and Fox B G 1966 *Science* **151** 75
[20] La Placa S and Bost P 1962 *Acta Crystallogr.* **15** 97
[21] Wang X B, Tian D C and Wang L 1994 *J. Phys.: Condens. Matter* **6** 10185
[22] Wang J Y and Zhou Y C 2004 *Phys. Rev.* B **69** 214111
[23] Ravindran P, Fast L, Korzhavyi P A, Johnnsson B, Wills J and Eriksson O 1998 *J. Appl. Phys.* **84** 4891
[24] Mattesini M and Matar S F 2002 *Phys. Rev.* B **65** 075110
[25] Hill R 1952 *Proc. Phys. Soc. Lond.* **65** 349
[26] Cynn H, Klepeies J E, Yoo C-S and Young D A 2002 *Phys. Rev. Lett.* **88** 135701
[27] Occelli F, Farber D L, Badro J, Arance C M, Teter D M, Hanfland M, Canny B and Couzinet B 2004 *Phys. Rev. Lett.* **93** 095502
[28] Grossman J C, Mizel A, Côté M, Cohen M L and Louie S G 1999 *Phys. Rev.* B **60** 6343
[29] Guo Y D, Cheng X L, Zhou L P, Liu Z J and Yang X D 2006 *Physica* B **373** 334
[30] Vajeeston P, Ravindran P, Ravi C and Asokamani R 2001 *Phys. Rev.* B **63** 045115
[31] Haines J, Léger J M and Bocquillon G 2001 *Annu. Rev. Mater. Res.* **31** 1
[32] Young A F, Sanloup C, Gregoryanz E, Scandolo S, Hemley R J and Mao H-K 2006 *Phys. Rev. Lett.* **96** 155501
[33] Jhi S-H, Ihm J, Louie S G and Cohen M L 1999 *Nature* **399** 132
Wu Z G, Chen X J, Struzhkin V V and Cohen R E 2005 *Phys. Rev.* B **71** 214103